

Phonon-assisted recombination in Fe-based spin LEDs

R. Mallory, M. Yasar, G. Itskos,* and A. Petrou

Department of Physics, SUNY at Buffalo, Buffalo, New York 14260, USA

G. Kioseoglou, A. T. Hanbicki, C. H. Li, O. M. J. van't Erve, and B. T. Jonker

Naval Research Laboratory, Washington, D.C. 20375, USA

M. Shen and S. Saikin†

Department of Electrical and Computer Engineering, Clarkson University, Potsdam, New York 13699, USA

(Received 21 October 2005; revised manuscript received 4 January 2006; published 6 March 2006)

The electroluminescence (EL) spectra from Fe/AlGaAs(*n*)/GaAs/AlGaAs(*p*) spin LEDs contain an e_1h_1 excitonic feature; in addition, they exhibit new features not present in the photoluminescence (PL) spectra, that are “satellites” or “replicas” of the exciton. These satellites are red shifted with respect to e_1h_1 by energies that are approximately equal to those of zone edge phonons in GaAs. The intensity of the replicas depends strongly on bias voltage. In the presence of a magnetic field the satellites become circularly polarized as σ_+ but their polarization is always lower than that of e_1h_1 . The satellites are interpreted as due to recombination processes that involve zone edge electrons that tunnel into the GaAs quantum well. These processes occur simultaneously with the emission of zone-edge phonons. Our interpretation is supported by a numerical simulation of the properties of electrons tunneling through an Fe/GaAs(*n*) Schottky barrier.

DOI: [10.1103/PhysRevB.73.115308](https://doi.org/10.1103/PhysRevB.73.115308)

PACS number(s): 78.60.Fi, 72.25.Hg, 72.10.Bg, 63.20.Dj

INTRODUCTION

During the last few years the spin light emitting diode¹ (spin LED) has emerged as a practical tool for the determination of spin injection efficiencies from spin polarizing semiconductor²⁻⁴ and metal contacts.⁵⁻⁹ Particular emphasis has been placed on Fe-based LEDs because Fe is a ferromagnet with a high Curie temperature, and thus a promising candidate for room temperature device applications.^{7,10} The band edge electroluminescence (EL) spectra from Fe/AlGaAs(*n*)/GaAs/AlGaAs(*p*)/GaAs(*p*) light emitting diodes (LEDs) consist of features associated with recombination processes that occur (a) in the quantum well (QW) and (b) in the GaAs buffer layer. The former involve electrons injected by the Fe contact that are captured by the GaAs quantum well; the latter involve injected electrons that travel past the QW and recombine in the GaAs(*p*) buffer layer. The circular polarization P_{circ} of the excitonic e_1h_1 feature is used to determine the spin polarization of the electrons in the QW. In addition to the e_1h_1 exciton, the EL contains new features below e_1h_1 , not present in the photoluminescence (PL) spectra. The new features appear at fixed energy shifts from e_1h_1 ; thus we will refer to them as “satellites” or “replicas” of the excitonic transition. Based on a numerical simulation of the properties of electrons tunneling through an Fe/GaAs(*n*) Schottky barrier we propose a model which explains the presence of the satellites as well as their characteristics.

EXPERIMENTAL

In this paper we discuss results from three spin-LEDs labeled as sample 1, 2, and 3. The samples were grown

by molecular-beam epitaxy (MBE) using interconnected growth chambers on *p*-type GaAs substrates. Samples 1 and 2 were grown on (100) oriented substrates, while sample 3 was grown on a (110) substrate. The structures' layer sequence is as follows. 5000 Å *p*-GaAs buffer/250 Å *p*-Al_{0.3}Ga_{0.7}As ($p=10^{18}$ cm⁻³)/250 Å undoped Al_{0.3}Ga_{0.7}As spacer/undoped GaAs quantum well of width $L_w/100$ Å undoped Al_{0.1}Ga_{0.9}As spacer/450 Å *n*-Al_{0.1}Ga_{0.9}As ($n=10^{17}$ cm⁻³)/150 Å *n*-Al_{0.1}Ga_{0.9}As transition layer/150 Å *n*-Al_{0.1}Ga_{0.9}As ($n=10^{19}$ cm⁻³)/125 Å Fe contact.

The well widths L_w are 125 Å for sample 1, 85 Å for sample 2, and 135 Å for sample 3. The samples were processed into surface emitting LEDs using conventional photolithography and chemical etching techniques. The Faraday geometry was employed for the magneto-optical studies. The diodes were placed in a variable temperature optical magnet cryostat. The emitted light was dispersed by a single monochromator equipped with a multichannel charge coupled device (CCD) detector. The EL spectra were analyzed as σ_+ (LCP) and σ_- (RCP) using a combination of quarter wave plate and linear polarizer placed before the spectrometer entrance slit. The degree of circular polarization of a particular spectral feature is defined as $P_{\text{circ}}=(I_+-I_-)/(I_++I_-)$, where I_+ (I_-) is the intensity of the σ_+ (σ_-) feature component.

RESULTS

The zero-field band edge EL spectrum from sample 1 (well width $L_w=125$ Å) recorded at $T=6$ K is shown in Fig. 1. The spectrum is a convolution of several peaks that correspond to different recombination channels. Deconvolution of the EL reveals the following features: X (at 12 414 cm⁻¹), a (at 12 330 cm⁻¹), X_B (at 12 222 cm⁻¹), $CB \rightarrow A$ (at

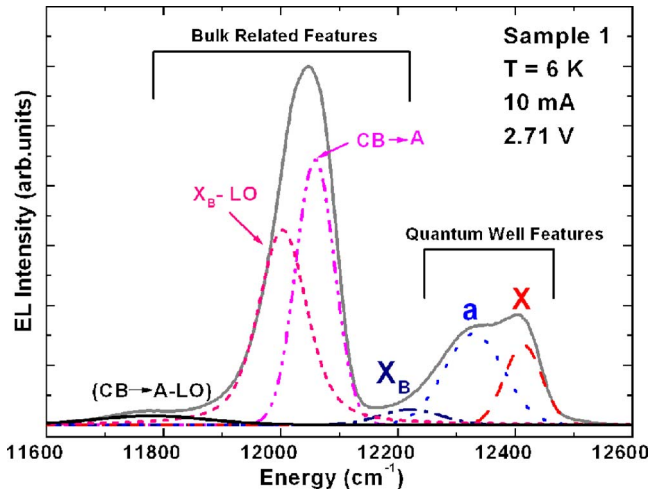


FIG. 1. (Color online) Zero field EL spectrum from sample 1 at $T=6$ K (gray solid line). The various spectral components have been line fitted as follows. (I) Quantum well features: X (long-dashed line); a (coarse dotted line). (II) Bulk related features: X_B (dashed-dotted line); $CB \rightarrow A$ (dashed-double dotted line); X_B-LO (short-dashed line); $(CB \rightarrow A)-LO$ (thin solid black line).

$12\,040\text{ cm}^{-1}$). Feature X is associated with the quantum well e_1h_1 exciton. The feature labeled “ X_B ” is identified as the bulk exciton from the GaAs buffer. The strong feature labeled “ $CB \rightarrow A$ ” is attributed to the conduction band \rightarrow acceptor transition from the GaAs(p) buffer. The identification of the latter is made on the basis of its energy^{11,12} and the fact that its position does not change in LEDs which incorporate quantum wells with different well widths.

Feature a is identified as an exciton satellite because it always has approximately the same energy shift with respect to the exciton in all (100) samples. In Fig. 1 we also include a line fitting of features X and a that yields an energy difference of 84 cm^{-1} . Feature a is present in all Fe LEDs and its relative intensity with respect to e_1h_1 varies greatly with bias voltage. For sample 1 this is illustrated in Fig. 2 where the e_1h_1 exciton (feature X) and its satellite (feature a) are shown for the current (voltage) range 2–20 mA (2.03–2.91 V). For low bias voltages feature a is clearly dominant over feature X . As the bias voltage is increased, feature a loses intensity while feature X becomes stronger. Similar behavior is observed in all samples. The circular polarization P_{circ} of features X and a from sample 1 is plotted as function of magnetic field B in Fig. 3. The polarization increases rapidly with B between $B=0$ and 2.5 T. At this magnetic field the out-of-plane magnetization of the Fe contact saturates and the remaining small slope of the P_{circ} versus B plot is due to the heavy hole magnetic field splitting.^{5,13} The behavior shown in Fig. 3 is consistent for all samples, i.e., the satellites always have a lower polarization than the e_1h_1 exciton.

In sample 2 (well width $L_w=85\text{ \AA}$) in which the e_1h_1 exciton occurs at a higher energy ($12\,560\text{ cm}^{-1}$), and therefore is well removed from the strong bulk ($CB \rightarrow A$) feature, we have been able to resolve additional satellites. The zero magnetic field EL spectrum of sample 2 at $T=6$ K is shown in Fig. 4. The excitonic feature has three satellites labeled as

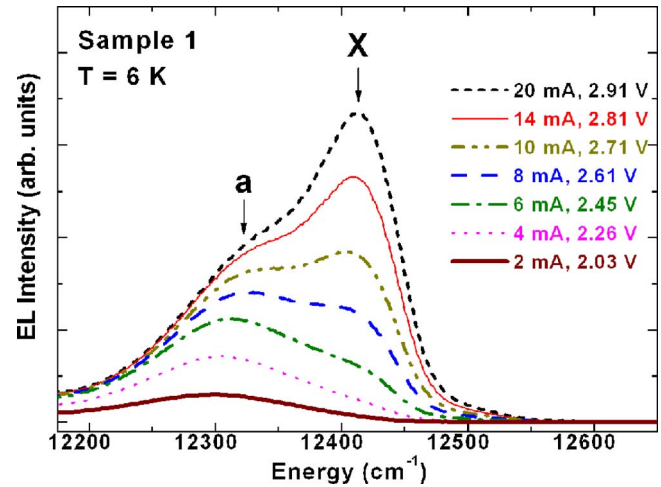


FIG. 2. (Color online) Zero field EL spectra at $T=6$ K from sample 1 in the vicinity of the quantum well exciton (features X and a) for different bias voltages: 2.03 V (heavy solid line), 2.26 V (fine dotted line), 2.45 V (dashed-dotted line), 2.61 V (long-dashed line), 2.71 V (dashed double dotted line), 2.81 V (light solid line), and 2.91 V (short dashed line).

“ a ,” “ b ,” and “ c ” at $12\,474\text{ cm}^{-1}$ (shift from e_1h_1 : 86 cm^{-1}), $12\,372\text{ cm}^{-1}$ (shift from e_1h_1 : 187 cm^{-1}), and $12\,278\text{ cm}^{-1}$ (shift from e_1h_1 : 282 cm^{-1}). In addition the spectrum contains four features associated with recombination in the bulk GaAs buffer (the exciton X_B , the $CB \rightarrow A$ transition, and their LO replicas). The energy shifts of satellites a , b , and c for sample 2 are suggestively close to the energies of the zone edge TA, LA, and LO phonons along the (100) direction in GaAs.^{14,15} Similar exciton satellites associated with zone edge TA, LA, and LO AlAs phonons have been observed in type-II GaAs/AlAs quantum wells.¹⁶ In this case the lower energy $X(\text{AlAs}) \rightarrow h_1(\text{GaAs})$ interband excitonic transition is forbidden by the crystal momentum conservation rule. Thus the recombination occurs simultaneously with the emission of TA, LA, and LO AlAs phonons.

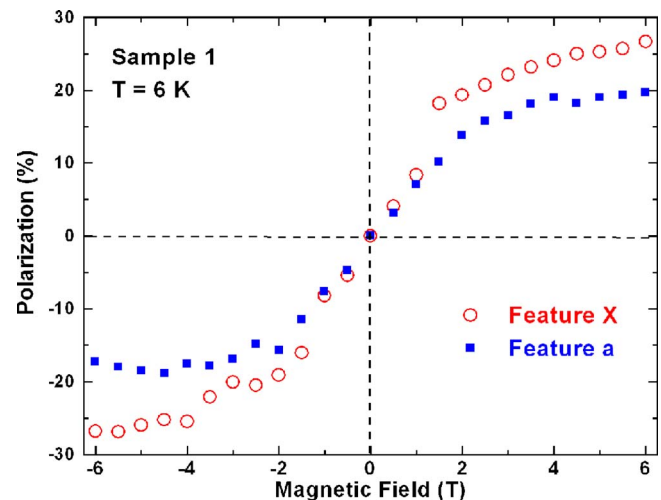


FIG. 3. (Color online) Circular polarization P_{circ} from sample 1 plotted as function of magnetic field B for feature X (open circles) and feature a (solid squares); $T=6$ K.

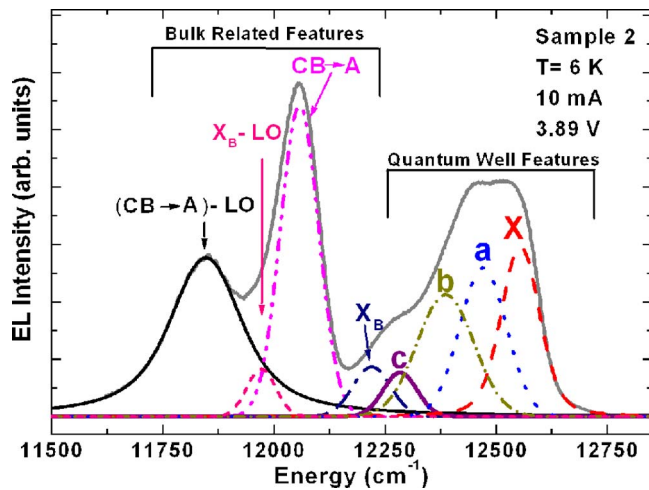


FIG. 4. (Color online) Zero field EL spectrum from sample 2 at $T=6$ K (gray solid line). The various spectral components have been line fitted as follows. (I) Quantum well features: X (long-dashed line), a (coarse dotted line), b (fine-dotted-dashed line), c (thick solid line). (II) Bulk related features: X_B (dashed-dotted line), $CB \rightarrow A$ (dashed-double dotted line), X_B-LO (short-dashed line), $(CB \rightarrow A)-LO$ (thin solid black line).

In order to verify that the connection of the EL satellites with the phonons is not a coincidence we have also investigated sample 3 which is grown on a (110) substrate. Waugh and Dolling reported two additional phonon modes propagating along the (110) direction.¹⁵ These modes were labeled as “IA” and “IIA,” respectively. Mode IA has a maximum frequency of 111 cm^{-1} close to the (110) zone edge at point K in the Brillouin zone; it also exhibits a maximum in the density of states at this energy. The zero field EL spectrum of sample 3 at $T=6$ K is given in Fig. 5. The e_1h_1 exciton (feature X) occurs at 12390 cm^{-1} and its satellite (feature a') at 12285 cm^{-1} , i.e., it exhibits an energy shift of 105 cm^{-1} rather than the 86 cm^{-1} shift observed in sample 2. We thus

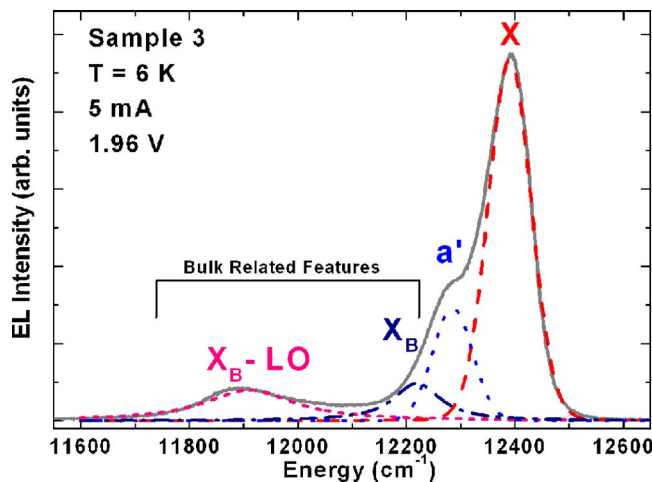


FIG. 5. (Color online) Zero field EL spectrum from sample 3 at $T=6$ K (gray solid line). The various spectral components have been line fitted as follows. (I) Quantum well features: X (long-dashed line), a' (coarse dotted line). (II) Bulk related features: X_B (dashed-dotted line); X_B-LO (short-dashed line).

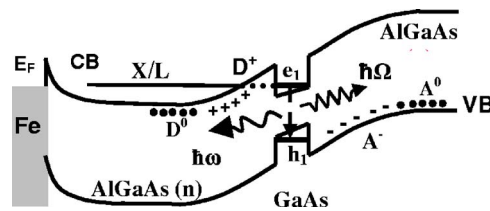


FIG. 6. (Color online) Schematic band diagram of the conduction and valence band edges for the $Fe/AlGaAs(n)/GaAs/AlGaAs(p)$ spin diodes used in this study under low bias conditions.

identify satellite a' in sample 3 as being associated with phonon mode IA. This differentiates the (110) from the (100) spin LEDs and provides convincing evidence about the connection of the EL exciton satellites with the phonons.

DISCUSSION

In the following discussion we present a mechanism that can explain the appearance and properties of the satellites in the EL spectra. The energy shifts of the satellites suggest that they are associated with electron-hole recombination processes accompanied by the simultaneous emission of a phonon close to the zone edge. Using crystal momentum conservation we conclude that the electrons involved with the satellite features have a high k vector. The proposed model is summarized in Fig. 6 in which we show a schematic diagram of the conduction and valence band edges in an $Fe/AlGaAs(n)/GaAs/AlGaAs(p)$ diode at low bias voltages. The strong bending of the bands in the vicinity of the GaAs QW is generated by the junction electric field. The band bending at the $Fe/AlGaAs(n)$ interface is due to the Schottky barrier potential. The horizontal line labeled “X/L” represents the X and L valleys. Electrons injected from the Fe contact are promoted into these valleys by the strong electric field of the Schottky barrier at the $Fe/AlGaAs(n)$ interface, as will be discussed in more detail in the next section. The satellites are attributed to the following processes: Electrons populating the upper valleys in the $AlGaAs(n)$ layer tunnel through the narrow triangular barrier to the left of the QW [at the $AlGaAs(n)/GaAs$ interface] into the e_1 conduction confinement subband of the well.^{17,18} Recombination can occur only if a zone edge phonon is simultaneously emitted in order to satisfy the conservation of crystal momentum. The energy of the emitted photons in these processes is equal to the energy e_1h_1 of the zero-phonon ground state exciton less the energy of the emitted phonon. Under flat band conditions (high bias voltage) the EL spectra are dominated by the zero-phonon e_1h_1 excitonic feature. The recombination process in this case involves electrons with k vector approximately equal to zero that reach the quantum well via the diffusive mechanism. Recombination associated with the near zero k -vector electrons does not require the emission of a phonon.

NUMERICAL SIMULATION

In this section we describe a numerical simulation of spin polarized electron injection through a (100) $Fe/GaAs(n)$

Schottky barrier. The objective is to characterize electron transport properties and spin dynamics in a metal/semiconductor structure near the Schottky barrier. The simulations have been carried out on an Fe/GaAs rather than an Fe/AlGaAs system because the material parameters required for the calculation in GaAs are readily available in the literature.

The numerical approach applied is an ensemble Monte Carlo scheme which has been modified to account for electron transport within three (Γ , X , and L) nonequivalent valleys in GaAs and also for the Fermi-Dirac distribution in the metal contact. In our model electrons traverse the Schottky barrier by tunneling.^{19,20} It is assumed that the potential barrier is one-dimensional, i.e., it does not affect electron momentum components in the barrier plane, and that tunneling occurs instantaneously. We assume that only spin majority electrons can tunnel through the Schottky barrier. This assumption is close to the results of first principles calculations.^{21,22} In the semiconductor part of the structure, transport within the three (Γ , X , and L) nonequivalent valleys is considered. After injection the electron motion is controlled by the electric field and scattering. The potential profile is calculated self-consistently at each time step of the simulation based on an electron distribution with boundary conditions specified by the applied voltage. Within the Fermi Golden Rule we take into account (a) intravalley scattering (by considering electron interactions with impurities, acoustic phonons, and optical polar phonons) and (b) intervalley scattering (by considering electron interactions with optical nonpolar phonons).²³ All the electrons are initially injected into the Γ valley and are then redistributed among the three valleys (Γ , X , and L) under the action of the Schottky barrier electric field and optical phonon scattering. The initial population of the Γ valleys is justified by the fact that the potential barrier is narrower for the Γ valley than it is for the X and L valleys. Thus we expect electrons to tunnel efficiently from the metal contact to the Γ valley. The simulated structure has the following characteristics: 3000 Å drain part doped at $n^+ = 2.5 \times 10^{18} \text{ cm}^{-3}$ /6700 Å channel with donor concentration $n = 2.5 \times 10^{16} \text{ cm}^{-3}$ /150 Å transition layer/150 Å of highly doped GaAs ($n^+ = 2.5 \times 10^{18} \text{ cm}^{-3}$)/ferromagnetic metal contact. In the model the doping profile near the Schottky barrier is similar to that of the LEDs studied; the absolute doping levels used in the simulation are lower due to the smaller bandgap of GaAs. The simulated structure does not include a quantum well even though experimentally the recombination takes place in such a well. This omission appreciably simplifies the model and reduces the number of model parameters. Though tunneling between 3D barriers and a quasi-2D QW has been studied thoroughly,^{17,18,24,25} only recently has the issue of spin filtering in nonmagnetic resonant tunneling structures been addressed.^{26,27} In our model we make the additional simplifying assumption that no spin filtering occurs during electron tunneling into the quantum well. The expectation is that the calculation qualitatively describes the properties of electrons in the spin LEDs under study in the region between the Schottky barrier and the GaAs quantum well.

The concentration of the injected electrons in the Γ ,

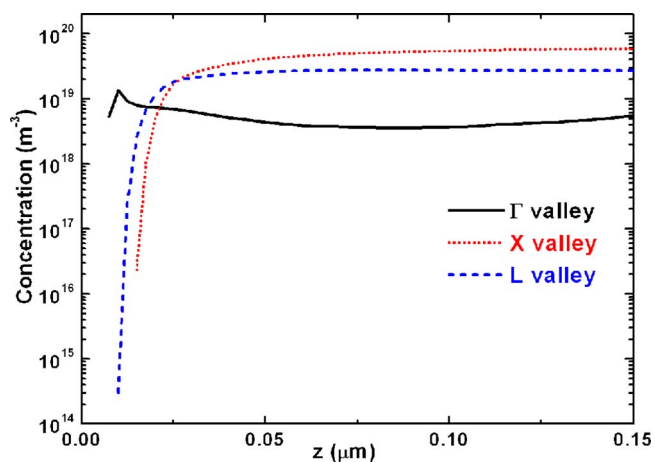


FIG. 7. (Color online) Results of the numerical simulation discussed in the text showing the electron concentration in the Γ , X , and L valleys plotted versus the distance z from the metal/semiconductor interface. The Γ , X , and L valleys are indicated by solid, dotted, and dashed lines, respectively.

X , and L valleys calculated for a bias voltage $V=2$ V as a function of distance z from the metal/semiconductor interface is shown in Fig. 7. At low temperatures electrons are injected by tunneling in a narrow energy range near the metal Fermi level.²⁸ The calculation shows that injected electrons are redistributed among the valleys very rapidly. Within a distance range of 30–300 nm the electron population in the upper valleys (X and L) is higher than that in the Γ valley. A similar pattern of electron distribution is obtained for different values of applied bias voltages within the 1.5–2.5 V range. This is consistent with previous studies of high field electron transport in GaAs.²⁹

From the results shown in Fig. 7 it is clear that the majority of the injected electrons in the vicinity of the GaAs quantum well populate the X and L valleys. Even though the calculation indicates that the L valleys are populated there is no convincing evidence in the EL spectra of a satellite with an energy shift of 62 cm^{-1} (i.e., the energy of the L valley TA phonon). It is possible that there are two components contained in feature “a” that are not resolved due to the width of the satellites and the proximity of the zone edge TA phonons at the X and L points of the Brillouin zone.

To evaluate spin dynamics of the injected electrons in our system we take into account the spin-orbit interaction.³⁰ The latter produces precessional spin dephasing in an ensemble of spin-polarized electrons.³¹ During the transport the electron spin precesses about a momentum-dependent axis. Electron momentum scattering randomizes the axis orientation and leads to spin dephasing. Near the bottom of the Γ , X , and L valleys the spin-orbit interaction Hamiltonian can be written as $H_{\text{SO}} = \vec{\Omega}(\vec{k}) \cdot \vec{\sigma}$.³² Here $\vec{\sigma}$ is the Pauli spin operator, \vec{k} is the electron wave vector, and $\Omega \sim k^3$ for the Γ valley and $\Omega \sim k$ for the upper (X and L) valleys. Within a given valley, the spin-orbit coupling coefficients are assumed energy independent and are taken from theoretical calculations.^{33,34}

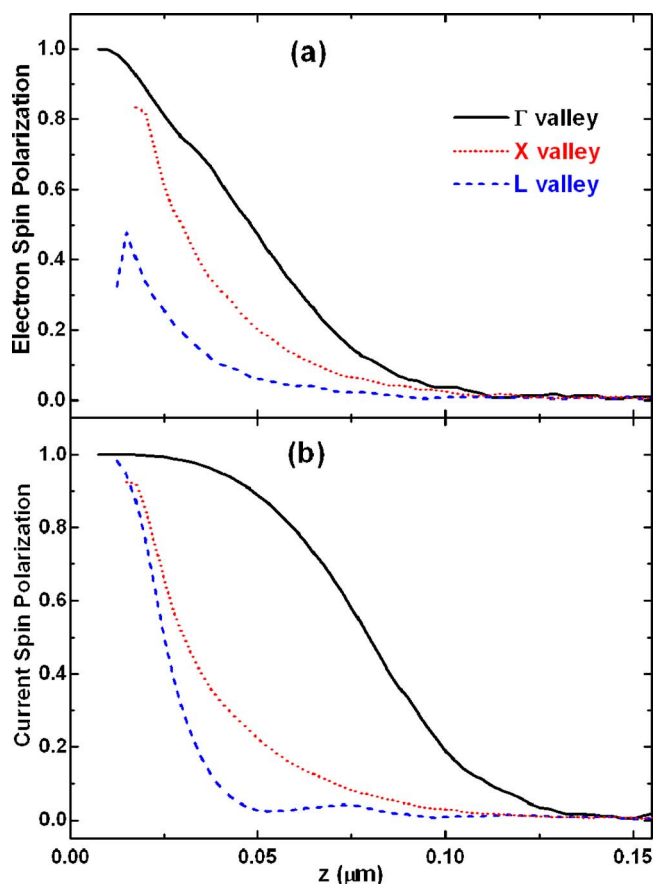


FIG. 8. (Color online) Results of the numerical simulation discussed in the text showing (a) magnitude of the electron spin polarization and (b) magnitude of the current spin polarization plotted versus the distance z from the metal/semiconductor interface for the Γ (solid line), X (dotted line), and L (dashed line) valleys.

Electron spin dynamics is characterized by two parameters:³⁵ (a) electron spin polarization $\vec{P}(z) = \langle \vec{s}_i \rangle_z$ and (b) current spin polarization $\vec{\alpha}(z) = \langle v_{zi} \vec{s}_i \rangle_z / \langle v_{zi} \rangle_z$. Here \vec{s}_i is the spin polarization of the i th electron, v_{zi} is the electron velocity component along the transport direction (z axis); averaging $\langle \cdots \rangle_z$ is taken over all electrons within a small element of thickness dz centered at z .

In Figs. 8(a) and 8(b) we plot the magnitude of the electron spin polarization and current spin polarization calculated at $T=6$ K as function of distance z at a bias voltage $V=2$ V. Initially, injected electrons are assumed to be 100% polarized along the z axis. Electron polarization and current spin polarization are calculated for electrons traversing the barrier in regions where electron concentration is high enough to obtain good statistics. Therefore, the polarization curves in Fig. 8 begin at some distance from the metal/semiconductor interface. From the two plots it can be seen that electron spin polarization and current polarization decay within a distance ~ 100 nm from the Fe/GaAs interface. In the upper valleys spin dephasing is more pronounced because of stronger spin-orbit coupling.³⁴ This trend is observed for applied voltages within the 1.5–2.5 V range. We have also considered electron spin precession in an external

magnetic field up to 2 T, but have found this effect to be small. Qualitatively our simulation model confirms the smaller circular polarization of the phonon satellites with some overestimation of spin scattering rates. The latter can be due to the assumption that spin-orbit coupling is independent of the electron energy within a given valley. The reduced polarization of the satellites can be qualitatively described by stronger spin scattering in the upper valleys. Three other mechanisms can also result in a lower circular polarization P_{circ} for the phonon satellites: (a) energy-dependent spin filtering at the Schottky barrier,²¹ (b) spin filtering during the tunneling from the three-dimensional AlGaAs(n) barrier into the quasi two-dimensional quantum well,²⁶ and (c) electron spin flip during phonon emission. None of these mechanisms have been considered in this simple model.

In a recent study of spin transport in lateral ferromagnet/semiconductor structures spin decay lengths up to $50 \mu\text{m}$ have been observed.³⁶ The dramatic difference in the spin decay lengths between the work of Crooker *et al.* and this study is attributed to the corresponding differences in device geometry. In the lateral geometry of Ref. 36 the electrons move away from the strong electric field region of the source Schottky barrier. In contrast, in our work the electrons always move under the Schottky barrier and thus experience a strong electric field. Finally, we would like to point out that the phonon satellites are present in the EL spectra of reference samples in which the magnetic Fe contact has been replaced by a nonmagnetic metal, indicating that phonon-assisted recombination does not depend on the contact material.

CONCLUSIONS

The excitonic (e_1h_1) feature in the EL spectra from Fe-based GaAs/AlGaAs spin LEDs is accompanied by one or more satellites which are red shifted with respect to e_1h_1 . The satellites dominate the spectra at low bias voltages but decrease in intensity as the bias voltage is increased. In the presence of a magnetic field the circular polarization P_{circ} of the satellites is consistently lower than that of e_1h_1 . The appearance of the satellites is attributed to recombination processes associated with near zone edge electrons that tunnel into the GaAs quantum well. The recombination is accompanied by the emission of near zone edge phonons in order to satisfy crystal momentum conservation. This model is supported by the results of a numerical simulation of spin polarized electron injection through an Fe/GaAs(n) Schottky barrier.

The presence of the satellites in the EL spectra is interesting from two points of view. The first is practical and is connected with the accurate determination of the spin injection efficiency in these devices.³⁷ At low bias voltages the phonon satellites dominate the EL spectra and can be easily misidentified as the zero-phonon e_1h_1 transition. Such an error would result in underestimating the spin injection efficiency of the device under study. The second reason is that in Fe spin LEDs we can distinguish unambiguously two types of electrons that contribute to the overall current. (a) Elec-

trons with near zero k vector associated with the zero-phonon e_1h_1 transition. (b) Electrons with the k vector close to the zone edge, associated with the phonon satellites. The two recombination channels have photon energies that can be easily resolved. Effectively in these devices a second quantum number (the electron k vector) has been added to the spin quantum number of the electron and could potentially be utilized for practical applications.

ACKNOWLEDGMENTS

The authors thank Ming-Cheng Cheng and Vladimir Privman for useful discussions. Work at SUNY Buffalo was supported by NSF (Grant No. ECS 0524403) and ONR (N000140610174). Work at NRL was supported by ONR (N0001404WX20052), DARPA SpinS program (K920/00), and core program at NRL. Work at Clarkson was supported by NSF (Grant No. DMR0121146)

*Present address: Physics Department, Imperial College, London, UK.

†Present address: Physics Department, University of California San Diego, San Diego CA 92093.

¹I. Zutic, J. Fabian, and S. Das Sarma, *Rev. Mod. Phys.* **76**, 323 (2004).

²R. Fiederling, M. Keim, G. Reuscher, W. Ossau, G. Schmidt, A. Waag, and L. W. Molenkamp, *Nature (London)* **402**, 787 (1999).

³B. T. Jonker, Y. D. Park, B. R. Bennett, H. D. Cheong, G. Kioseoglou, and A. Petrou, *Phys. Rev. B* **62**, 8180 (2000).

⁴Y. Ohno, D. K. Young, B. Beschoten, F. Matsukura, H. Ohno, and D. D. Awschalom, *Nature (London)* **402**, 790 (1999).

⁵A. T. Hanbicki, B. T. Jonker, G. Itskos, G. Kioseoglou, and A. Petrou, *Appl. Phys. Lett.* **80**, 1240 (2002).

⁶A. T. Hanbicki, O. M. J. van't Erve, R. Magno, G. Kioseoglou, C. H. Li, B. T. Jonker, G. Itskos, R. Mallory, M. Yasar, and A. Petrou, *Appl. Phys. Lett.* **82**, 4092 (2003).

⁷X. Jiang, R. Wang, R. M. Shelby, R. M. Macfarlane, S. R. Bank, J. S. Harris, and S. S. P. Parkin, *Phys. Rev. Lett.* **94**, 056601 (2005).

⁸J. Strand, B. D. Schultz, A. F. Isakovic, C. J. Palmstrom, and P. A. Crowell, *Phys. Rev. Lett.* **91**, 036602 (2003).

⁹H. J. Zhu, M. Ramsteiner, H. Kostial, M. Wassermeier, H. P. Schonherr, and K. H. Ploog, *Phys. Rev. Lett.* **87**, 016601 (2001).

¹⁰C. H. Li, G. Kioseoglou, O. M. J. van't Erve, M. E. Ware, D. Gammon, R. M. Stroud, B. T. Jonker, R. Mallory, M. Yasar, and A. Petrou, *Appl. Phys. Lett.* **86**, 132503 (2005).

¹¹A. M. White, P. J. Dean, D. J. Ashen, J. B. Mullin, M. Webb, B. Day, and P. D. Greene, *J. Plasma Phys.* **6**, L243 (1973).

¹²F. Willman, W. Dreybrodt, M. Bettini, E. Bauser, and D. Bimberg, *Phys. Status Solidi B* **60**, 751 (1973).

¹³H. A. Nickel, G. Kioseoglou, T. Yeo, H. D. Cheong, A. Petrou, B. D. McCombe, D. Broido, K. K. Bajaj, and R. A. Lewis, *Phys. Rev. B* **62**, 2773 (2000).

¹⁴C. Patel, T. J. Parker, H. Jamshidi, and W. F. Sherman, *Phys. Status Solidi B* **122**, 461 (1984).

¹⁵J. L. T. Waugh and G. Dolling, *Phys. Rev.* **132**, 2410 (1963).

¹⁶B. A. Wilson, C. E. Bonner, R. C. Spitzer, R. Fischer, P. Dawson, K. J. Moore, C. T. Foxon, and G. W. t'Hooft, *Phys. Rev. B* **40**,

1825 (1989).

¹⁷E. A. Rezek, N. Holonyak, B. A. Vojak, and H. Shichijo, *Appl. Phys. Lett.* **31**, 703 (1977).

¹⁸B. A. Vojak, N. Holonyak, R. Chin, E. A. Rezek, R. D. Dupuis, and P. D. Dapkus, *J. Appl. Phys.* **50**, 5835 (1979).

¹⁹S. Saikin, M. C. Cheng, and M. Shen, cond-mat/0512414 (unpublished).

²⁰M. Shen, S. Saikin, and M. C. Cheng, *J. Appl. Phys.* **96**, 4319 (2004).

²¹O. Wunnicke, P. Mavropoulos, R. Zeller, P. H. Dederichs, and D. Grundler, *Phys. Rev. B* **65**, 241306(R) (2002).

²²X. G. Zhang and W. H. Butler, *J. Phys.: Condens. Matter* **15**, R1603 (2003).

²³M. V. Fischetti and S. E. Laux, *DAMOCLES Theoretical Manual* (IBM Research Division, Yorktown Heights, NY, 1995).

²⁴V. J. Goldman, D. C. Tsui, and J. E. Cunningham, *Phys. Rev. B* **36**, 7635 (1987).

²⁵N. S. Wingreen, K. W. Jacobsen, and J. W. Wilkins, *Phys. Rev. Lett.* **61**, 1396 (1988).

²⁶M. M. Glazov, P. S. Alekseev, M. A. Odnoblyudov, V. M. Chistyakov, S. A. Tarasenko, and I. N. Yassievich, *Phys. Rev. B* **71**, 155313 (2005).

²⁷T. Koga, J. Nitta, H. Takayanagi, and S. Datta, *Phys. Rev. Lett.* **88**, 126601 (2002).

²⁸R. Stratton, *Tunneling in Schottky Barrier Rectifiers* (Plenum Press, New York, 1969).

²⁹J. Pozela and A. Reklaitis, *Solid-State Electron.* **23**, 927 (1980).

³⁰G. Dresselhaus, *Phys. Rev.* **100**, 580 (1955).

³¹M. I. D'yakonov and V. I. Perel, *JETP Lett.* **33**, 1053 (1971).

³²E. L. Ivchenko and G. E. Pikus, *Superlattices and Other Heterostructures. Symmetry and Optical Phenomena* (Springer, New York, 1997).

³³M. Cardona, N. E. Christensen, and G. Fasol, *Phys. Rev. B* **38**, 1806 (1988).

³⁴J. M. Jancu, R. Scholz, G. C. La Rocca, E. A. de Andrade Silva, and P. Voisin, *Phys. Rev. B* **70**, 121306(R) (2004).

³⁵Z. G. Yu and M. E. Flatte, *Phys. Rev. B* **66**, 235302 (2002).

³⁶S. A. Crooker, M. Furis, X. Lou, C. Adelman, D. L. Smith, C. J. Palmstrom, and P. A. Crowell, *Science* **309**, 2191 (2005).

³⁷B. T. Jonker, A. T. Hanbicki, Y. D. Park, G. Itskos, M. Furis, G. Kioseoglou, A. Petrou, and X. Wei, *Appl. Phys. Lett.* **79**, 3098 (2001).